Preparation and Crystallization of Poly(ethylene terephthalate)/SiO₂ Nanocomposites by *In-Situ* Polymerization

Yongzhe Yang, Hong Xu, Hongchen Gu

National Key Laboratory of Nano/Micro Fabrication Technology, Key Laboratory for Thin Film and Microfabrication of Ministry of Education, Institute of Micro and Nano Science and Technology, Shanghai Jiaotong University, Shanghai 200030, China

ABSTRACT: Poly(ethylene terephthalate) (PET)/SiO₂ nanocomposites were prepared by *in situ* polymerization. The dispersion and crystallization behaviors of PET/SiO₂ nanocomposites were characterized by means of transmission electron microscope (TEM), differential scanning calorimeter (DSC), and polarizing light microscope (PLM). TEM measurements show that SiO₂ nanoparticles were well dispersed in the PET matrix at a size of 10–20 nm. The results of DSC and PLM, such as melt-crystalline temperature, half-time of crystallization and crystallization kinetic constant, suggest that SiO₂ nanoparticles exhibited strong nucleating effects. It was found that SiO₂ nanoparticles could effectively promote the nucleation and crystallization of PET, which may be due to reducing the specific surface free energy for nuclei formation during crystallization and consequently increase the crystallization rate. © 2006 Wiley Periodicals, Inc. J Appl Polym Sci 102: 655–662, 2006

Key words: crystallization; *in situ* polymerization; nanocomposites; poly(ethylene terephthalate)

INTRODUCTION

Crystallization process of poly(ethylene terephthalate) (PET) has recently been widely reinvestigated due to the increasing technological interest. It is well-known that PET is a semicrystalline thermoplastic with excellent mechanical, physical, and chemical properties, including excellent chemical and heat resistance, high stiffness and strength, and good dimensional stability. These properties make PET an attractive high performance polymer for engineering plastic applications in areas of electronics, transportation, construction, and consumer products.[1] However, PET applied as an engineering plastic for injection molding is rather limited, due to its slow crystallization rate and large cycle time compared with poly(butylenes terephthalate).[2–7]

Because of the cost advantage offered by PET, many efforts have been made to search for nucleation agents. Ionomers, polymers, inorganic, and organic compounds have been reported as the candidates.[2–6] A survey of the recent literature indicates an apparent consensus, according to which sodium benzoate has been used as an effective nucleation agent for PET.[8–10] However, it was also observed that PET was degraded by the salt under processing conditions.

In this study, we have demonstrated that it is possible to control the crystallization behavior of PET by inorganic nanoparticles, which have been paid little attention before. Table I shows some recent polymer-based nanocomposites prepared via: (a) the sol–gel technique; (b) *in-situ* intercalative polymerization; (c) *in-situ* polymerization; (d) melt mixing.[11] Direct melt mixing method has received only limited effects on crystallization, due to the high tendency of agglomeration of nanoparticles during blending.[12–14] Conversely, *in situ* polymerization has been proved to provide nanocomposite with novel properties.[15–20] This study adopted *in situ* polymerization for realizing real nanocomposites by nanoscale. The methodology consists of dispersing the inorganic nanoparticles into the monomers; then the mixture is polymerized by adding the catalyst and stabilizing agent under certain condition. To promote the compatibility between organic/inorganic components and improve the homogeneous dispersion of the nanoparticles into the polymeric matrix, the nanoparticles can be further treated with a coupling agent. The crystallization of PET, both unnucleated and nucleated with SiO₂ nanoparticles, has been studied under isothermal and nonisothermal conditions by DSC and PLM.

TABLE I
Recent Polymer-Based Nanocomposite Systems[11]

Systems	Uses
Sol–gel technique	
Polycaprolactone (PCL)/silica(TEOS)	Bone-bioerodible polymer composites for skeletal tissue repair
Polyimide/silica (TEOS)	Micro-electronics
PMMA/silica	Dental application, optical devices
Polyethylacry (PEA)/silica	Catalysis support, stationary phase for chromatography
Poly(amide-imide)/TiO_2	Composite membranes: gas-separation applications
In situ interculative polymerization	
iPP/organoclay	Improved properties
Starch/organo-modified montmorillonite	Enhanced barrier properties
Nylon/organ-modified montmorillonite	Improvement of structural, mechanical, thermal and barrier characteristics without significant loss in clarity or strength
In situ polymerization	
Nylon 6/silica and $CaCO_3$	Improvement of structural, mechanical, thermal and barrier characteristics without significant loss in clarity or strength
Polyimide/AlN	Materials for microelectronics with reduced thermal expansion coefficient and moisture absorption
PMMA/$CaCO_3$	Biocompatible materials and optical devices
PET/SiC	Improved properties
Melt mixing	
Polyethylene/graphite	Applications in electrical or thermal conductors, electromagnetic interference shields, self-lubricated materials
Poly(lactic acid)/organo clay	Improved properties
Polystyrene/organo clay	Engineering plastics

EXPERIMENTAL

Materials

Nano-SiO_2 with average particle size of 10 nm was supplied by Yuda Chemical Co. (Zhejiang, China). Ethylene glycol (EG), terephthalic acid, trimethyl phosphate, Sb_2O_3 (as catalyst), and organosilane coupling agent A-187 were supplied by Chemical Reagents Co. (China).

Preparation of the SiO_2/ethylene glycol sol

About 2.4 g of organosilane coupling agent A-187 was dissolved in 100 mL water and heated at 60–70°C for 20 min. The solution was added dropwise to 100 g 25 wt % SiO_2/H_2O sol, maintaining the flow rate at 10 mL/min. Then, the modified SiO_2 was transferred from water to ethylene glycol by rotatory evaporation. The dispersion of 25 g of modified SiO_2 in a 100 mL of ethylene glycol solution was added to another 100 mL of ethylene glycol, which was heated at 80–120°C. Similarly, the flow rate was controlled at 10 mL/min. The mixture was stirred vigorously for 30 min.

Preparation of PET/SiO_2 nanocomposites by *in situ* polymerization

PET pellets with varied content of SiO_2 were prepared by the PTA route. In a 5-L cylindrical reactor, 1 kg of EG (16.1 mol) and varied content of SiO_2 were placed; the mixture was stirred for 0.5 h at room temperature.

Then, 2 kg of terephthalic acid (12.0 mol), a few drops of trimethyl phosphite, and some Sb_2O_3 were added, with vigorous stirring to obtain a homogeneously dispersed system. The mixture was then heated in nitrogen atmosphere from room temperature to 250–260°C under a pressure of 0.3 MPa. After completed esterification, the pressure was reduced to air pressure to emit the water generated during the esterification. Then, the polymerization was carried on at 260–270°C under a pressure of 200–300 Pa to drain out the excess EG. Afterward, the pressure was controlled to less than 40 Pa. After 1–2 h polycondensation, the melting polymer was extruded through an orifice at nitrogen pressure of 0.3 MPa and cooled with water.

Characterization

PET/SiO_2 nanocomposite specimens were sliced at −80°C with an Ultracut Uct microtome. A transmission electron microscope operated at 75 kV was used to obtain images of the nanocomposites specimens. Before TEM experiment, specimens were annealed in a vacuum oven at 100°C for 1 week to remove moisture completely.

The crystallization behaviors of the samples were examined using PerkinElmer differential scanning calorimetry system DSC-2C. During isothermal crystallization experiments, samples were heated at 50°C/min to 300°C, and maintaining there for 5 min to eliminate the thermal and shear history effects, and then

TABLE II
Fundamental Properties of Pure PET
and Its Nanocomposites

Specimen	Intrinsic viscosity (dL/g)	—COOH (mol/10^3 kg)	Lucency	B
Pure PET	0.68	15.3	86.2	1.4
PET/0.5 wt % SiO₂	0.68	14.8	86.5	1.6
PET/1.0 wt % SiO₂	0.69	14.1	90.6	1.2
PET/1.5 wt % SiO₂	0.68	14.5	85.3	1.1
PET/2.0 wt % SiO₂	0.68	15.6	83.4	1.5
PET/2.5 wt % SiO₂	0.68	16.0	82.2	1.1
PET/3.0 wt % SiO₂	0.69	13.4	88.6	1.3

quenched to the desired isothermal crystallization temperature. The samples were maintained at the crystallization temperature for 40 min during which the crystallization characteristics were recorded. During nonisothermal crystallization experiments, samples were heated at 50°C/min to 300°C, maintaining 300°C for 5 min to eliminate the thermal and shear history effects, and then cooling at 20°C/min to 100°C. The peak corresponding to the maximum in the heat flow rate was taken as the crystallization temperature (T_c).

Melt nucleation and crystallization of PET and its nanocomposites were measured using a LEICA-DMLP polarizing light microscope (PLM) equipped with a Linkam-TMS94 heating stage. The specimen was sandwiched between two glass slips, melted at 300°C for 5 min to eliminate thermal history, cooled to 234°C for isothermal crystallization, and then maintained there for 20 min.

RESULTS AND DISCUSSION

Fundamental properties of PET nanocomposites

The fundamental properties (intrinsic viscosity, carboxylate end group concentration, lucency, color parameter) of pure PET and PET nanocomposites are listed in Table II. The intrinsic viscosities of the samples are approximately equal because the polymerizations were controlled by melt viscosities. It can be found from Table II that the other parameters of PET/SiO₂ nanocomposites are also consistent with those of pure PET, which means that the introduction of SiO₂ nanoparticles had no significant effect on the polymerization process.

Dispersion of nanoparticles in PET/SiO₂ nanocomposites

It is well-known that the dispersion of nanoparticles in the polymer matrix has a significant impact on the
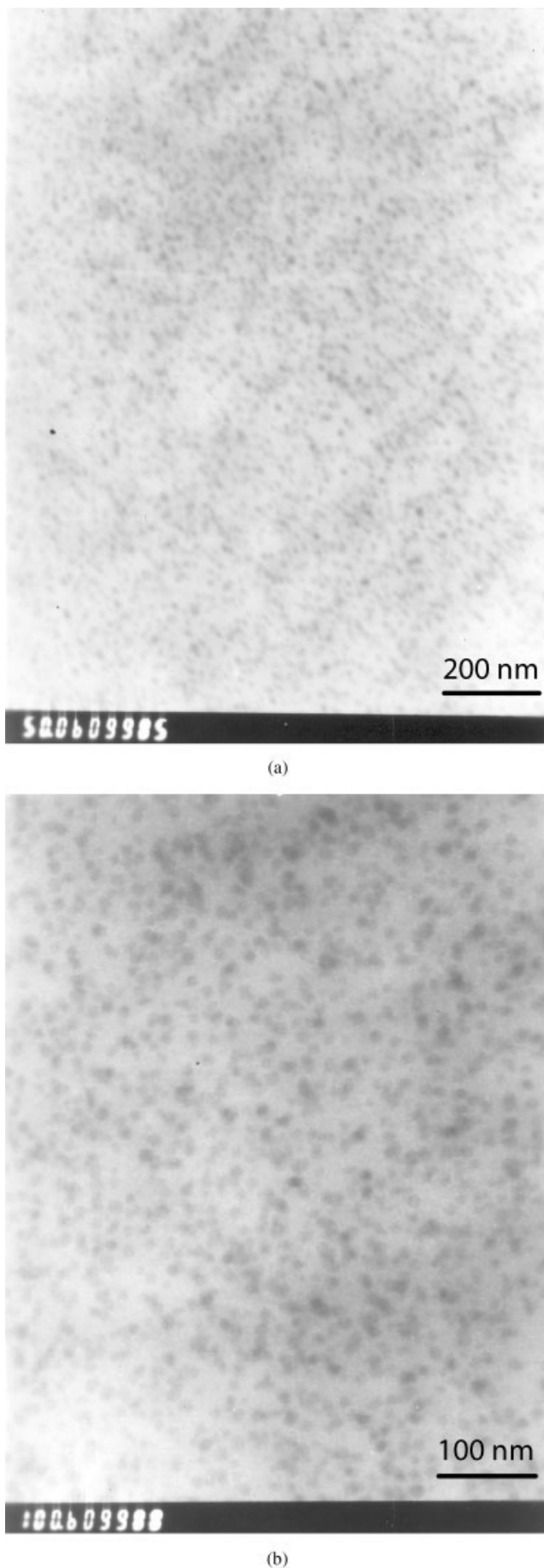
Figure 1 TEM photographs of PET/2.0 wt % SiO₂ nanocomposite prepared by *in situ* polymerization (a) ×50,000 (b) ×100,000.

Specimen	T_g (°C)	T_c (°C)	T_c^* (°C)	T_m (°C)	H_c^* (J/g)	$(T_c^* - T_c)$ (°C)	ΔT_{sc} (°C)
Pure PET	67.7	135.0	158.0	242.9	29.0	23.0	84.9
PET/0.5 wt % SiO$_2$	68.9	138.0	186.5	248.2	33.9	48.5	61.7
PET/1.0 wt % SiO$_2$	69.4	138.1	193.5	248.0	33.0	55.4	54.5
PET/1.5 wt % SiO$_2$	69.7	138.5	195.8	249.0	35.0	57.3	53.2
PET/2.0 wt % SiO$_2$	70.4	137.2	200.0	249.0	33.5	62.8	49.0
PET/2.5 wt % SiO$_2$	70.8	135.0	202.9	249.0	33.7	67.9	46.1
PET/3.0 wt % SiO$_2$	71.0	130.0	202.7	251.0	34.8	72.7	48.3

T_g, the glass transition temperature; T_c, the cold-crystalline temperature; T_c^* the melt-crystalline temperature; T_m, the melting temperature; H_c^*, the melt-crystalline heat; $T_c^* - T_c$, the extent of crystalline temperature; $\Delta T_{sc} = (T_m - T_c^*)$, the degree of supercooling.

properties of composites.[21–24] As the nanoparticles have a strong tendency to agglomerate, homogeneous dispersion of the nanoparticles in the polymer has been considered as a difficult process. A good dispersion may be achieved by surface modification of the nanoparticles under an appropriate processing condition.[25] In this work, a novel approach has been utilized to disperse nanoparticles in the PET matrix. Figure 1 shows TEM images of PET-based nanocomposite having 2.0 wt % of SiO$_2$ nanoparticles, where the dark areas represent the SiO$_2$ particles and gray/white areas represent the PET matrix. It is clearly seen that SiO$_2$ nanoparticles have been dispersed fairly well. The sizes of SiO$_2$ particles range between 10 and 20 nm.

Nonisothermal crystallization

A summary description of crystallization behavior of pure PET and its nanocomposites is shown in Table III. The temperature T_c at which an exothermic peak occurs during DSC heating course (cold crystallization peak) and T_c^* during the cooling course (melt crystallization peak) were measured.

Comparison of the modified samples with pure PET shows that the increase in melt-crystalline temperature T_c^* with the increase of SiO$_2$ content is obvious. The extent of increase in T_c^* is by about 28.5–44.9°C. The increase can be attributed to the incorporation of effective nucleation agent SiO$_2$ and its satisfactory dispersion in the PET matrix. It is well-known that the molecular chains of pure PET present higher inflexibility and less mobility. As a result, both crystallization rate and nucleation rate are very slow, corresponding to the low T_c^*. When SiO$_2$ nanoparticles are added to the PET matrix, it enhances the crystallization rate of PET by providing large numbers of nucleation sites. In other words, SiO$_2$ nanoparticles induce a growth of crystalline layer around their surface. The molecular chains can crystallize at high temperature and tend to transform perfectly at the same time. Both

crystallization rate and nucleation rate are very fast, corresponding to the high T_c^*.

Figure 2 shows the DSC cooling scans of nonisothermal crystallization from melt state for PET and its nanocomposites. The temperatures of peaks vary with the content of SiO$_2$ over a range of 0–3.0 wt % and their shapes become much narrower than that of pure PET. The effect of SiO$_2$ nanoparticles on crystallization is reaching its maximum at approximately 2.5 wt % whose crystallization peak is narrowest, but not at expectably 3.0 wt %. As shown in Figure 2, the differences in the onset and peak temperature of crystallization curves between 2.5 wt % and 3.0 wt % SiO$_2$ content nanocomposites are not very distinct. However, the crystallization exotherm of PET/3.0 wt % SiO$_2$ is less narrow than that of PET/2.5 wt % SiO$_2$ mainly because of a queue in the crystallization curve at low temperatures. This may be due to a larger
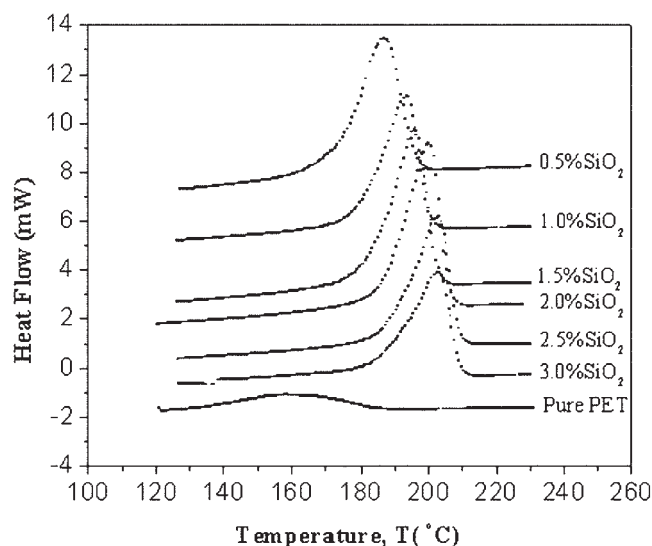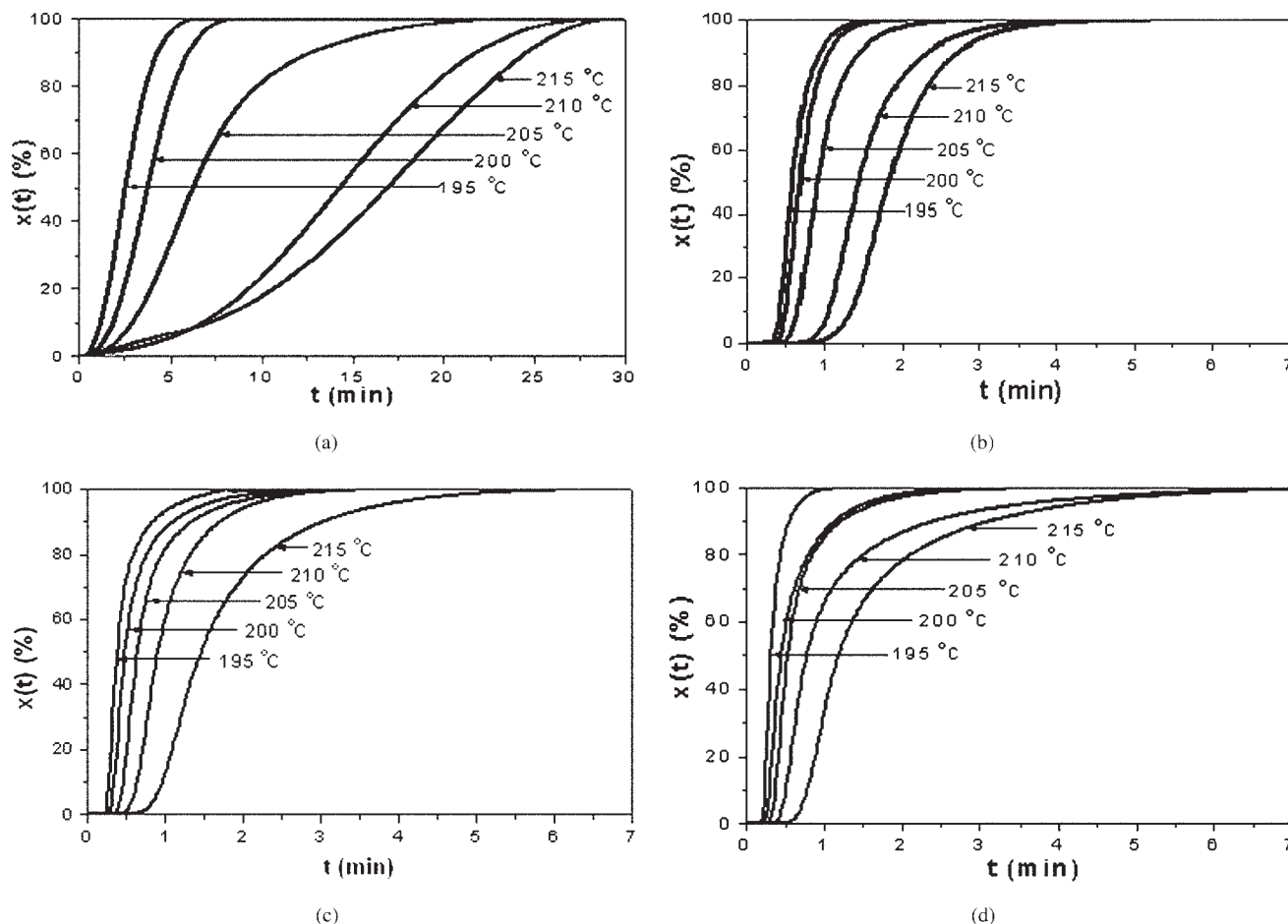

Figure 2 DSC cooling scans of nonisothermal crystallization from melt state for pure PET and PET/SiO$_2$ nanocomposites.

Figure 3 Plots of isothermal crystallization for pure PET and PET/SiO$_2$ nanocomposites (a) $x(t)$ versus t of pure PET; (b) $x(t)$ versus t of PET/1.0 wt % SiO$_2$; (c) $x(t)$ versus t of PET/2.0 wt % SiO$_2$; (d) $x(t)$ versus t of PET/3.0 wt % SiO$_2$.

reduction in crystallization rate, probably caused by a larger crystal impingement arising from a higher number of growing spherulites.

From Table III, the cold-crystalline temperature T_c of pure PET is about 135.0°C, in agreement with previous reported data.[26] At a small addition of SiO$_2$ nanoparticles, there is an obvious increase in T_c, while excessive SiO$_2$ nanoparticles result in the decrease in T_c. The maximum in T_c can be observed in the PET/1.5 wt % SiO$_2$ nanocomposite. There may be two quite different ways in which SiO$_2$ influences T_c: (i) SiO$_2$ nanoparticles act as balls, which can decrease interactivity between molecular chains of PET. This function of lubrication makes the molecular chains more flexible and mobile; (ii) the introduction of SiO$_2$ nanoparticles with high surface activity produce an obstacle on the molecular chains movement, which will also reduce the tendency for molecular chains to be crystallized, since they may react or chelate with functional groups (—COOH, —OH at the end, and —O—(CO)) along the PET chains. This bridging function increases compatibility between the PET matrix and SiO$_2$ nanoparticles. At present, we still cannot verify whether

both mechanisms operate concomitantly and which one dominates.

The change in T_c and T^*_c might imply the influence of SiO$_2$ on the crystallization of PET. The values of $T^*_c - T_c$ in nanocomposites are obviously 25.5–49.7°C larger than those in pure PET. This implies that PET/SiO$_2$ nanocomposites have excellent performance for injection molding.

In programmed cooling, the crystallization temperature reflects the overall crystallization rate attributed to the combined effects of nucleation and growth. Thus, the degree of supercooling ($\Delta T_{sc} = T_m - T^*_c$) may be used to measure the crystallizability of pure PET and its nanocomposites; that is, the smaller the ΔT_{sc}, the higher the overall crystallization rate. The ΔT_{sc} values for the PET/SiO$_2$ nanocomposites are smaller, by 23.2–38.8°C, than those of pure PET (84.9°C), and the PET/2.5 wt %SiO$_2$ exhibits the smallest ΔT_{sc} (46.1°C). The result again reveals that the overall crystallization rate for the PET/SiO$_2$ nanocomposites is higher than that of pure PET.

From these findings, it can be concluded that SiO$_2$ nanoparticles have a strong heterogeneous nucleation

effect on PET, which offer enormous surface area and hence give rise to higher crystallization temperature and greater crystallization rate of PET during nonisothermal crystallization.

Isothermal crystallization

To analyze the isothermal crystallization kinetic data of the PET nanocomposites, we adopt the well-known Avrami equation.[27,28]

$$x(t) = 1 - \exp(-kt^n) \tag{1}$$

where $x(t)$ is the relative crystallinity, which is defined to be the volume fraction of polymer crystallized at time t. $x(t)$ is derived by integrating the crystallization exotherm (H_c) according to the DSC graph by the following equation:

$$x(t) = \frac{\int_0^t \frac{dH_c(t)}{dt} dt}{\int_0^{t=\infty} \frac{dH_c(t)}{dt} dt} \tag{2}$$

k is kinetic constant, and n is Avrami exponent, which depends on the mechanism of nucleation and the form of crystal growth. We can obtain a linear relation between $\log[-\ln(1-x(t))]$ and $\log t$ by changing the form of eq. (1).

$$\log[1 - \ln(1 - x(t))] = \log k + n \log t \tag{3}$$

Figure 3 shows the plots of $x(t)$ versus t for pure PET and its nanocomposites. Avrami exponent, kinetic constant calculated from isothermal crystallization are listed in Table IV.

On the basis of the classical crystal-nucleation theory, the nucleation is initiated by large-amplitude, localized fluctuations of some order parameter, such as density, leading to the appearance of small regions of the stable crystallizable phase.[29–31] When these regions are larger than some critical size, they will grow and eventually crystallize. However, the nature of such fluctuation has not been clarified. Phenomenologically, we can observe a transient time, the so-called induction period from amorphous state. In Table IV, the apparent increase in induction time (t_{ind}) with the increase in the crystallization temperature may well be simply due to the slowing-down of the overall crystallization process (nucleation and growth). Patkar and Jabarin report that this behavior of t_{ind} is due to the decrease in the nucleation rate at temperatures near melting point.[32] Kenny and Maffezzoli report that this delay is only representative of the induction
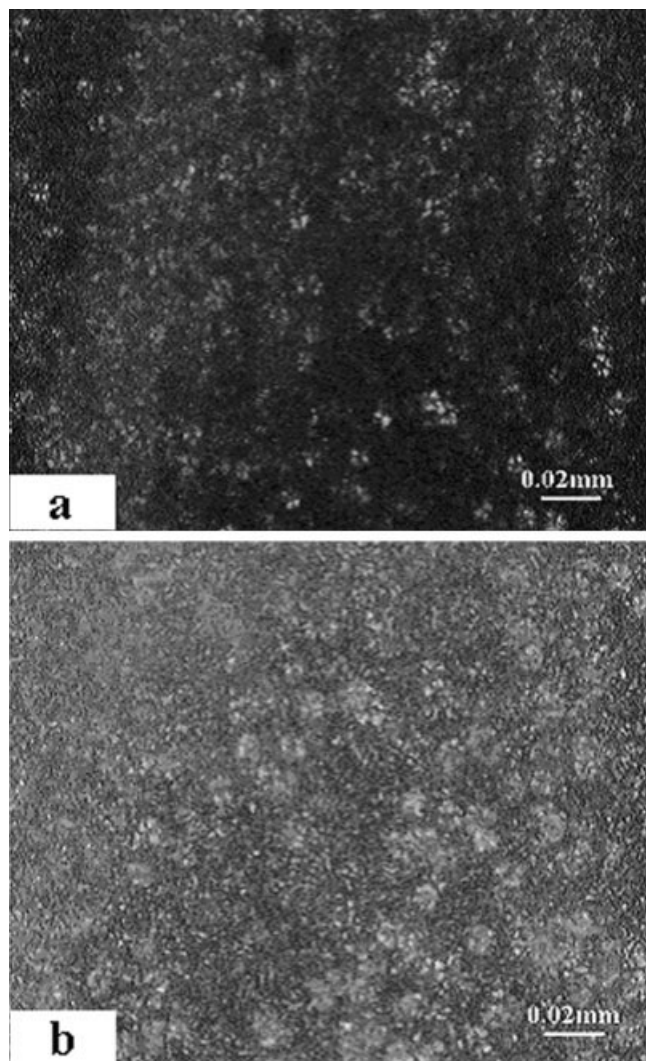
TABLE IV
Parameters of the Isothermal Crystallization of Pure PET and PET/SiO₂ Nanocomposites

Specimen	T_{iso} (°C)	t_{ind} (min)	$t_{1/2}$ (min)	n	$\log k$ (min⁻ⁿ)
Pure PET	215	0.68	17.57	2.72	−3.00
	210	0.62	14.83	2.62	−2.00
	205	0.56	7.80	2.60	−1.70
	200	0.50	4.18	2.41	−1.10
	195	0.48	3.03	2.20	−0.80
PET/1.0 wt % SiO₂	215	0.50	1.94	3.45	−0.44
	210	0.48	1.44	3.20	0.12
	205	0.37	0.88	3.00	0.70
	200	0.35	0.68	2.60	1.06
	195	0.30	0.56	2.35	1.10
PET/2.0 wt % SiO₂	215	0.45	1.47	3.00	−0.11
	210	0.37	0.90	2.86	0.65
	205	0.30	0.64	2.62	1.11
	200	0.25	0.48	2.37	1.27
	195	0.20	0.38	2.35	1.65
PET/3.0 wt % SiO₂	215	0.40	1.18	2.90	0.25
	210	0.32	0.77	2.56	0.82
	205	0.27	0.52	2.44	1.28
	200	0.22	0.45	2.33	1.44
	195	0.18	0.31	2.24	1.92

T_{iso}, the isothermal crystallization temperature; t_{ind}, the induction time of crystallization; $t_{1/2}$, the half time of crystallization; n, the Avrami exponent; k, the kinetic constant.

time associated with the crystal nucleation.[33] The large number of nuclei provided by the SiO₂ induces a large amount of crystallites to grow simultaneously, overweighing the effect of high surface free energy. There is a marked decrease in the induction time from 0.50 to 0.22 min between the pure PET and PET/SiO₂ nanocomposites at 200°C.

The Avrami exponent n depends on the mechanism of the nucleation as well as the growth geometry, which is usually an integer between 1 and 4 for different crystallization mechanisms. However, it has also been observed that n is a fraction due to the secondary crystallization or the crystal perfection. Based on the results in Table IV, the Avrami exponent n for constant SiO₂ concentration increases as a function of the temperature selected for crystallization. The n of pure PET with a narrow spread in values changes from 2.72 to 2.20 (with T_{iso} = 195–215°C), which are quite consistent with that reported by Chou and Chang but lower than that reported by Hobbs and Pratt.[34,35] For pure PET, its growth dimensions should predominantly be a two-dimensional growth, according to the definition of the Avrami exponent.[36,37] After introduction of SiO₂ nanoparticles, the n values are obviously higher than those of pure PET and are located between 3.45 and 2.24. For PET nanocomposites, its growth dimension should be two-dimensional or three-dimensional growth. This means that the addition of SiO₂ influences the mechanisms of growth of PET crystallites.

temperature and reflects that $t_{1/2}$ is strongly dependent on composition and crystallization temperature.[40] In contrast, Huang and Chang found $t_{1/2}$ changed exponentially with decreasing crystallization temperature.[41]

Morphology of the PET spherulites

Figures 4 and 5 show the PLM images of isothermal crystallization for pure PET and its nanocomposite. The pure PET forms a normal spherulitic structure with a size of 5–10 μm [Fig. 4(a)], while the diameter of spherulites of the nanocomposite is as small as 1 μm [Fig. 5(a)] at the same crystallization temperature (234°C) and time (3 min). As time goes on, the pure PET forms a larger spherulitic structure with a size of 15–20 μm [Fig. 4(b)]. However, the change in the diameter of spherulites of the nanocomposite is very unconspicuous, even hard to distinguish [Fig. 5(b)]. It

Figure 4 Morphologies of PET crystallizing at 234°C (×400) (a) 3 min; (b) 4 min.

Figure 5 Morphologies of PET/1.0 wt % SiO$_2$ crystallizing at 234°C (×400) (a) 3 min; (b) 4 min.
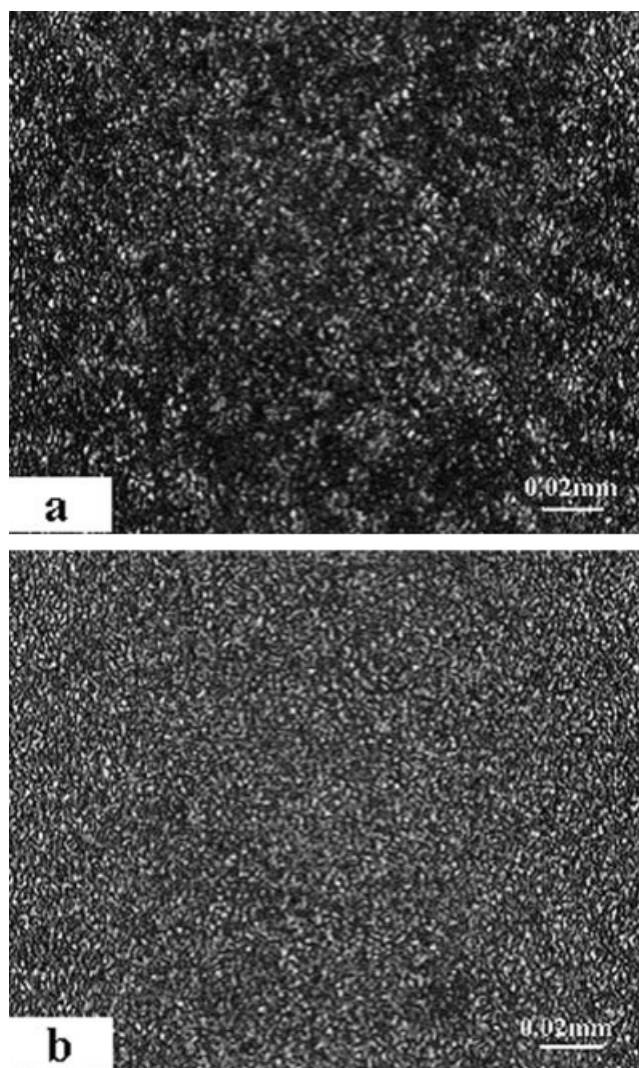
The kinetics constant k determines both the nucleation and the growth processes. From Table IV, it can be found that the k is extremely sensitive to crystallization temperature, which decreases with increasing crystallization temperature. According to Supaphol, this is only valid when the crystallization temperature is within the range where nucleation mechanism is the rate-determining step.[38,39] At the same temperature, the kinetics constant k of modified samples is about 78–1770 times larger than that of pure PET, indicating that SiO$_2$ is very effective as nucleation additive.

Table IV shows the effect of SiO$_2$ nanoparticles content on the half-time of PET crystallization ($t_{1/2}$) at different temperature. PET and PET/SiO$_2$ nanocomposites show a very noticeable linear decrease in $t_{1/2}$ as the decrease of crystallization temperature, indicating that the rate of crystallization is faster when the crystallization temperature is lower. This is consistent with the nucleation control of crystallization at high

is clear that the introduction of SiO_2 nanoparticles greatly affects the size of the PET spherulites. A great number of nucleus generated from SiO_2 simultaneously grow in a limit space and lead to the formation of small spherulites.

CONCLUSIONS

In this study, PET/SiO_2 nanocomposites were prepared by *in situ* polymerization. This method allows obtaining a homogeneous dispersion of the SiO_2 particles. The addition of SiO_2 results in an increase in crystallization rate and in a reduction of the spherulite size and the surface free energy for nucleus formation. All the crystallization parameters (T_c, T^*_c, n, k and $t_{1/2}$) were found to be sensitive to the content of SiO_2 within the explored range. The extent of increase in T^*_c is by about 28.5–44.9°C. The crystallization kinetics constants of PET/SiO_2 nanocomposites are about 78–1770 times larger than those of the pure sample. With the addition of nucleating agent SiO_2, smaller and more PET spherulites were observed.

References

1. Reinsch, V. E.; Rebendfeld, L. J Appl Polym Sci 1994, 52, 649.
2. Gunter, B.; Zachmann, H. G. Polymer 1983, 24, 1008.
3. Lu, X. F.; Hay, J. N. Polymer 2001, 42, 9423.
4. Maiti, S. N.; Mahapatro, P. K. J Appl Polym Sci 1991, 42, 310.
5. Maiti, P.; Okamoto, M. Macromol Mater Eng 2003, 288, 440.
6. Linin, L. J Appl Polym Sci 1999, 71, 1133.
7. Haubruge, H. G.; Jonas, A. M.; Legras, R. Macromolecules 2004, 37, 126.
8. Przygockiw, W.; Lochowicz, A. J Appl Polym Sci 1995, 19, 2683.
9. Legras, R.; Dekonick, J. M. Polymer 1986, 27, 109.
10. Zhu, P. P.; Ma, D. Z. Eur Polym J 2000, 36, 2471.
11. Avella, M.; Errio, M. E. Appl Organomet Chem 2001, 15, 435.
12. Alexandre, M.; Dubois, P. Mater Sci Eng 2000, 28, 1.
13. Chang, J. H.; Kim, S. J. Polymer 2004, 45, 919.
14. Wu, Y. P.; Ma, Y.; Wang, P. Q.; Zhang, L. Q. Macromol Mater Eng 2004, 289, 890.
15. Taniguchi, A.; Cakmak, M. Polymer 2004, 45, 6647.
16. Avella, M.; Errico, M. E.; Martuscelli, E. Nano Lett 2001, 1, 213.
17. Hwang, S. H.; Paeng, S. W.; Kim, J. Y.; Huh, W. Polym Bull 2003, 49, 329.
18. Wang, D.; Zhu, J.; Yao, Q.; Wilkie, C. A. Chem Mater 2002, 14, 3837.
19. Lebaron, P. C.; Wang, Z.; Pinnavia, T. J. Appl Clay Sci 1999, 12, 11.
20. Davis, C. H.; Mathias, L. J.; Gilman, J. W.; Schiraldi, D. A.; Schields, J. R. J Polym Sci Part B: Polym Phys 2002, 40, 2661.
21. Kansy, J.; Consolati, G.; Dauwe, C. Phys Chem 2000, 58, 427.
22. Petrovis, Z. S.; Javmi, L.; Waddon, A.; Banhegi, G. J Appl Polym Sci 2000, 76, 2272.
23. Rong, M. Z.; Zhang, M. Q.; Zheng, Y. X.; Zeng, X. M. Polymer 2001, 42, 3301.
24. Tang, Y.; Hu, Y.; Zhang, Z.; Wang, Z. Z.; Gui, Z.; Chen, Z. Y.; Fan, W. C. Macromol Mater Eng 2004, 289, 191.
25. Chan, C. M.; Wu, J. S.; Li, J. X.; Cheung, Y. K. Polymer 2002, 43, 2981.
26. Bian, J.; Ye, S. R.; Feng, L. X. J Polym Sci Part B: Polym Phys 2003, 41, 2135.
27. Avrami, M. J Chem Phys 1939, 7, 1103.
28. Avrami, M. J Chem Phys 1940, 8, 212.
29. Carmen, A.; Miren, L.; Jeanette, G.; Carmen, U. Compos Struct 2003, 62, 291.
30. Kelton, K. F. Solid State Physics; Academic Press: New York, 1991.
31. Imai, M.; Kaji, K.; Kanaya, T.; Sakai, Y. Phys B: Condens Matter 1995, 213, 718.
32. Patkar, M.; Jabarin, S. A. J Appl Polym Sci 1993, 471, 749.
33. Kenny, J. M.; Maffezzoli, A. Polym Eng Sci 1991, 31, 607.
34. Chou, R. M.; Chang, C. C.; Yu, T. L.; Tseng, Y. H.; Wu, M. J Polym Int 2001, 50, 213.
35. Hobbs, S. Y.; Pratt, C. F. Polymer 1975, 16, 462.
36. Wunderlich, B. Macromolecular Physics; Academic Press: New York, 1976.
37. Sperling, L. H. Introduction to Physical Polymer Science; Wiley: New York, 1986.
38. Supaphol, P. Thermochim Acta 2001, 370, 37.
39. Supaphol, P.; Spruiell, J. E. J Appl Polym Sci 2000, 75, 337.
40. Mandelkern, L. Crystalling of Polymers; McGraw-Hill: New York, 1964.
41. Huang, J. M.; Chang, F. C. J Polym Sci Part B: Polym Phys 2000, 38, 934.